REPORT DOCUMENTATION PAGE

Form Approved
OMB No. 0704-0188

1. AGENCY USE ONLY (Leave Blank)	2. REPORT DATE	3. REPORT TYPE AND DATES COVERED
	4/1/2003	Final, 3 Sep 2002 through 2 Mar 2003

4. TITLE AND SUBTITLE
Compact Intermediate-Temperature Fuel Cells

5. FUNDING NUMBERS
DAAD 19-02-C-0081

6. AUTHOR(S)
Yipeng Sun

7. PERFORMING ORGANIZATION NAME(S) AND ADDRESS(ES)
NuVant Systems, Inc.
10 W. 33rd St., 127
Chicago, IL60616

8. PERFORMING ORGANIZATION REPORT NUMBER

9. SPONSORING/MONITORING AGENCY NAME(S) AND ADDRESS(ES)
U.S. Army Research Office
P.O. Box 12211
Research Triangle Park, NC 27709-2211

10. SPONSORING/MONITORING AGENCY REPORT NUMBER
44179.1-CH-STI

11. SUPPLEMENTARY NOTES

12a. DISTRIBUTION/AVAILABILITY STATEMENT
Approved for public release; distribution unlimited.

12b. DISTRIBUTION CODE

13. ABSTRACT (Maximum 200 words)
"Report developed under STTR contract" for topic "ARMY02-T008"

In Phase I, we demonstrate the feasibility of making supported electronically insulating, proton conducting inorganic thin films on metal hydride foils for intermediate temperature fuel cell electrolytes. Free standing, all inorganic composite membranes consisting of 2 – 20 um inorganic films on 25 um Pd foil have been successfully prepared and used as proton conducting membrane for intermediate fuel cell application. On the contrary, it is very difficult to prepare a mechanically strong inorganic electrolyte membrane with the same thickness using conventional methods. The fuel cell based on the supported membranes shows complete tolerance to 5% CO balanced hydrogen with considerable stability at 250°C. We also demonstrated that Pd coated V foils are viable candidates for replacement of Pd as the supported structure for proton conducting electrolytes.

14. SUBJECT TERMS
STTR report

15. NUMBER OF PAGES
21

16. PRICE CODE

17. SECURITY CLASSIFICTION OF	18. SECURITY CLASSIFICTION OF THIS	19. SECURITY CLASSIFICTION OF	20. LIMITATION OF ABSTRACT

Table of Contents

1 Introduction

There is currently a pressing need for high energy density, high reliability small power systems for both military and civilian applications. Military operations face a trade-off between the weight of batteries and the weight of food, water, and essential gear that can be carried by soldiers. Soldier portable power is now reliant on lithium-thionyl chloride primary batteries, which will most likely be replaced by rechargeble lithium ion batteries as that technology improves over the next 2-3 years. Battlefield recharging of these (probably 50 W) secondary batteries will require high energy density power systems, which can run on liquid fuel in the 200-500 W range. In the civilian market, problems with grid power reliability have stimulated the need for reliable, environmentally friendly back up power systems. In these applications the cost per watt is a less important figure of merit than the energy density and the reliability. All of these applications promise a ripe entry point for fuel cells, which in principle can deliver very high energy densities as well as other advantages (clean operation, portability) [1].

The practical development of polymer electrolyte membrane (PEM) fuel cell systems faces several tough technical problems: (1) the operating temperature is limited by the organic proton conducting membrane, which is usually held below 100^{o}C to avoid dehydration. At this low temperature, CO catalyst poisoning is a very serious issue. In order to reduce the CO content in the reformate fuel to less than 50 ppm, a fuel processor system, which consists generically of a high temperature (800-900^{o}C) steam reformer, a low temperature (200-250^{o}C) water gas shift (WGS) unit, and a low temperature partial oxidation (PROX) unit, is needed. These extra components add cost, weight, and complexity to the system; (2) the polymer membrane need to be fully hydrated to have good proton conductivity, and this adds the complexity of a water-management system; (3) the WGS and PROX units cannot respond quickly to transient power demand, which leads to the production of CO "spikes" and poisoning of the downstream fuel cell anode catalyst.

The solution to the above-mentioned problems, we believe, is a robust, proton conducting, inorganic membrane that requires little or no water for proton transport. The composite membrane we are developing is based on electronically insulating proton conductors (EIPC's) supported on a thin sheet of metal foil. The known materials properties of the components of the membrane (as well as our preliminary tests) indicate that it can run at 250–400ºC. It is well known that increasing the temperature will serve to mitigate the catalyst problems of PEM fuel cells. The activation energy for oxidation of methanol or CO at Pt alloy anodes is in the range of 10-15 kcal/mol, which translates to an approximately tenfold increase in rate for every increment of 70^{o}C [2]. Thus, the quest for better catalysts should be augmented by the search for higher temperature electrolyte systems. Phosphoric acid fuel cells (PAFCs) do not require a PROX unit because they operate at 200^{o}C. Although CO is not a fuel at 200^{o}C, it is not a poison. However, PAFCs suffer from corrosion and cathode stability problems linked to the phosphoric acid electrolyte, and PAFC stacks have a longer pitch than membrane fuel cells because of the liquid electrolyte. The situation with the liquid-feed DMFC is worse, because in addition to catalyst poisoning, there are significant problems with fuel crossover and water management. Poly(benzimidazole) (PBI) membranes offer an alternative to Nafion and could allow cell temperatures to rise to 150-200^{o}C. However, PBI work is in the early research stage and the problems of catalysis, methanol crossover, and water management remain unsolved.

Other reasons exist for increasing the fuel cell operating temperature, even when using pure H_2. At high efficiencies (high cell voltage), the polarization at the anode can be less than 30 mV, yet the cell voltage is hundreds of mV below the thermodynamic value because of cathode polarization. The four-electron oxygen reduction kinetics would improve substantially if higher temperature electrolyte systems were employed.

2 Experimental sections

2.1 Materials

2.1.1 Ammonium Polyphosphate

Ammonium polyphosphate is prepared by the reaction of polyphosphoric acid with urea [3]. Polyphosphoric acid was prepared by dissolving phosphorus pentoxide into 85% phosphoric acid with the atomic ratio H/P = 1. An excess amount of urea was added slowly into the melt of polyphosphoric acid with stirring at 150°C. The crude polyphosphoric acid was purified by dissolving into hot water and then being precipitated by adding an equal volume of methanol.

2.1.2 BCN18

The nominal composition of the BCN18 used in this study is $Ba_3Ca_{1.18}Nb_{1.82}O_{8.73}$. In a typical synthesis process, stiochiometric amount of $BaCO_3$, $CaCO_3$ and Nb_2O_5 were mixed, milled and compacted into an alumina crucible. The mixture were heated at 10°C/min to 850°C, held there 2 hours to decompose the carbonates, then ramped at 10°C/min to 1450°C and held there for 16 hrs.

2.2 Coating techniques

2.2.1 Air spray method for ammonium polyphosphate/silica

80wt% ammonium polyphosphate and 20wt% 400 nm silica were stirred in methanol for two days before sprayed onto a clean 25 μm palladium foil using an airbrush. The coated foil was sintered in ammonium atmosphere at 390ºC for 1 hr to melt and mix ammonium polyphosphate and silica. The desired thickness and loading of composite materials can be achieved by repeating spraying and sintering steps.

2.2.2 Sol-gel method for BCN18

2.2.2.1 Preparation of BCN18 sol

1. Weigh 4 g of 2, 4 pentanedione ($CH_3COCH_2COCH_3$) in a clean, dry vial; add 1 g $Nb(OEt)_5$, gently shake well, close cap, leave at room temperature for 15 min.
2. Weigh 1.32 g $Ba(OAC)_2$, add 13 g acetic acid, vigorously stir.
3. Add solution (2) into solution (1), keep stirring.
4. Add 3 g water into the mixture. The solution becomes clear after a few minutes.
5. Add 0.32 g $Ca(OAC)_2$ into above solution, stir for another half hour.

2.2.2.2 Dip-coating

The clean Pd foil was immersed in the BCN18 sol for 1 min before pulling out. The pulling rate is roughly 1.3 cm/min. The coated foil was dried at room temperature for 15 min, and then transferred to a tubular furnace at 400ºC for half hour, and 650ºC for half hour. The multilayer film was

prepared by repeating above-mentioned steps. Finally, the membrane with desired number of layers was calcined at 650ºC overnight.

2.2.2.3 Solution-particle method for BCN18

BCN18 bulk was first ball milled for 2 days. 0.5 g of fine powder was then mixed with 0.5 g of BCN18 sol, and stirred for 2 days. The well-dispersed BCN18 slurry was dropped onto the freshly cleaned Pd foil and the excess slurry was spun off at 5000 rpm for 30 seconds. As-deposited BCN18 film was dried at room temperature for 2 hr before sintering at 650ºC for 1 hr.

2.3 Instruments

2.3.1 Fuel cell assembly and test stand

Figure 1 shows the assembly of the intermediate temperature fuel cell. A proton conducting metal foil coated with a thin layer of electronically insulting proton-conducting (EIPC) material is sandwiched between 2 catalyzed gas diffusion layers. The resulting MEA is placed between high temperature PTFE gaskets. The assembly is held together with alignment pins.

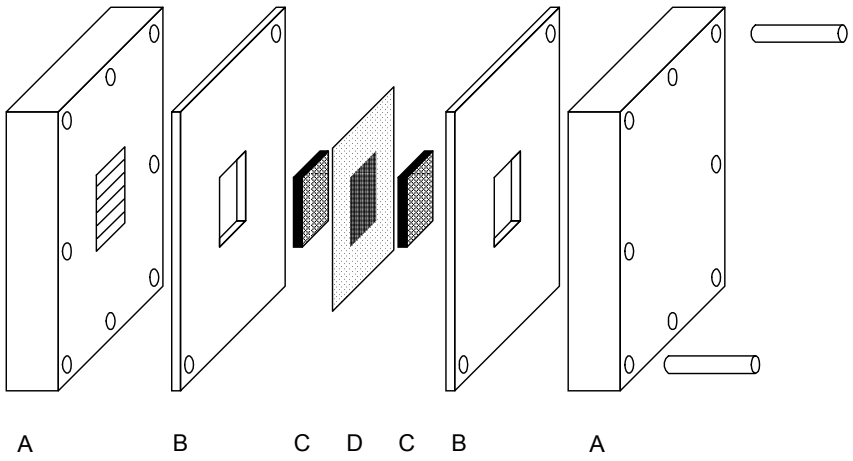

Fig. 1 Intermediate temperature fuel cell assembly.

Figure 2 shows the gas flow diagram and heating system. The fuel cell blocks are placed between two heating plates with process temperature up to 650°F. The 5-way valve enables change of fuel between H_2, H_2/1%CO and H_2/5%CO.

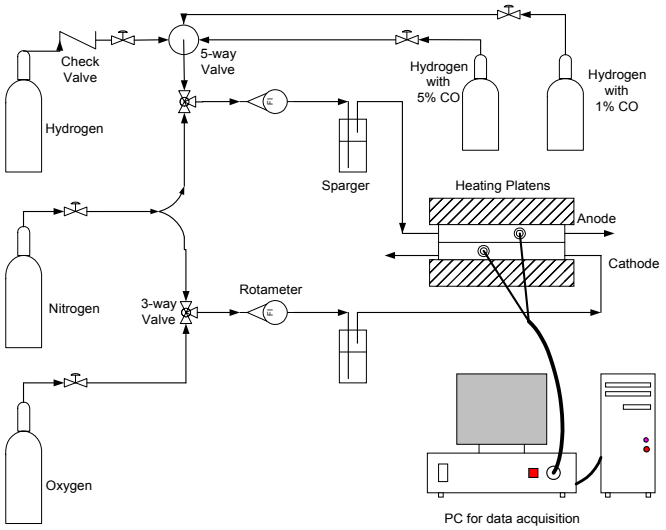

Fig. 2 Gas flow diagram and heating system.

2.3.2 GC setup for hydrogen permeability study

The key feature of the GC setup shown in Figure 3 is that it uses the same heating condition as that used in fuel cell testing. The membrane is positioned into the fuel cell block, which is placed between the heating plates. Initially, N_2 will be purged through both anode and cathode inlet. After the assembly is heated to a preset temperature, H_2 will then be delivered to the anode inlet. The cathode exhaust will be analyzed by GC.

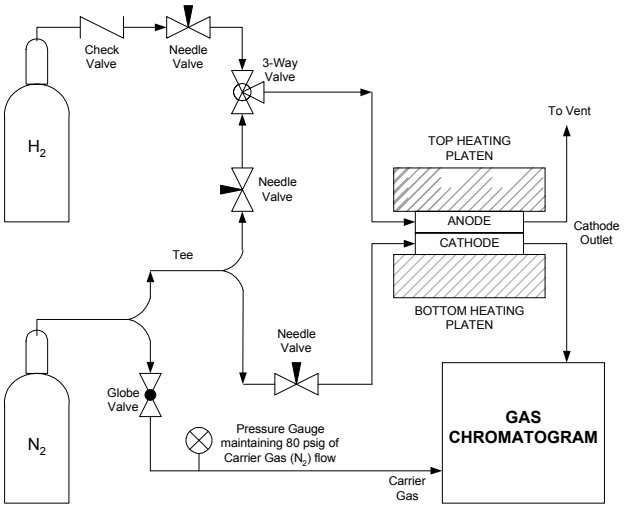

Fig. 3 Setup for hydrogen permeability study..

3 Results and discussion

3.1 Ammonium polyphosphate as EIPC material

3.1.1 Thermal analysis of ammonium polyphosphate

Figure 4 shows the thermogravimetric analysis (TGA) of ammonium polyphosphate, which was carried out with TA Instruments TGA 2050 apparatus using O_2 as the carrier gas. The analysis shows that the sample is free of moisture and is stable in an oxidizing atmosphere till about 250°C. Past this temperature it gradually loses volatile products. The principal loss mechanism is likely to be ammonia loss and dehydration.

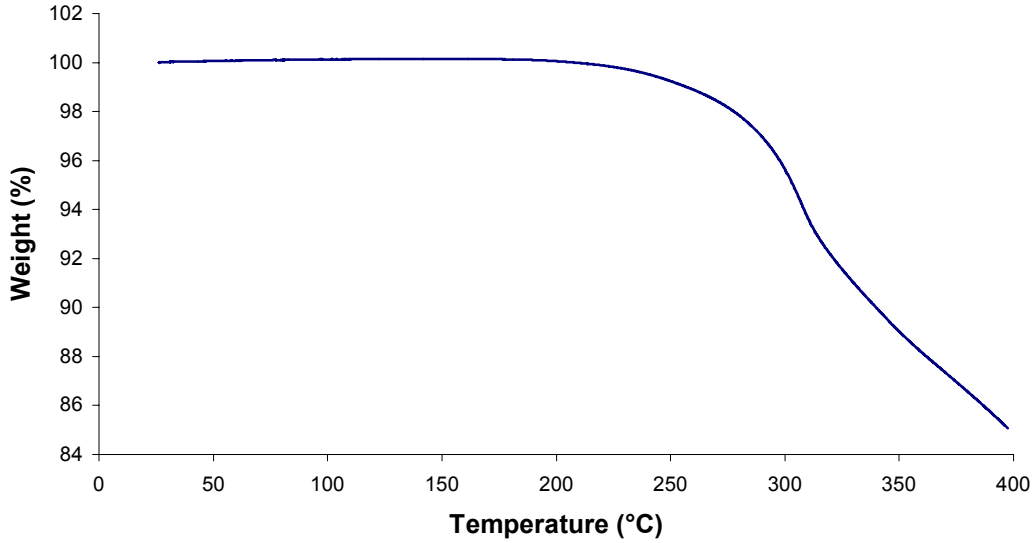

Fig. 4 Thermal Gravimetric Analysis (TGA) of Clariant ammonium polyphosphate in an oxidizing atmosphere

Figure 5 shows the thermogravimetric analysis (TGA) of pure ammonium polyphosphate and ammonium polyphosphate /silica at 250°C. The temperature was ramped to 250°C at 5°C/min and held there for 24 hr. Pure ammonium polyphosphate lost almost 10% of mass in 24 hour. The weight loss is fast in the first 10 hour (ca. 0.93%/hr) and slowed down thereafter (0.1%/hr). The original white powder turned into a hard, transparent gel after the heating, and the gel is easily dissolved in water, indicating the formation of polyphosphoric acid. All of this suggests loss of ammonia. The maximum mass loss of ammonia is ca. 17% for pure ammonium polyphosphate (NH_4PO_3). Therefore only part of ammonia has lost. It remains unknown what percentage of water was lost during the heating process.

Weight loss of ammonium polyphosphate/silica is ca. 5%, and most of weight loss (4%) happened in the first three hour. The original gray powder remained relatively unchanged after the heating, although part of it stuck to the pan, indicating the existence of pure ammonium polyphosphate. This phenomenon is different from what we observed for the ammonium polyphosphate/silica coatings after the fuel cell operation, in which the entire coatings changes from gray to white. The theoretical maximum weight loss is ca. 9% for the ammonium polyphosphate/silica mixture. Therefore only part of ammonia was lost.

In comparison, we studied the weight loss of the mixture of ammonium polyphosphate/silica and 20% Pt. We want to determine if the Pt catalyst on the cathode side is catalyzing a decomposition reaction. In this case, we see that the TGA weight loss is almost 10%. This is much higher than the 5% TGA weight loss with pure ammonium polyphosphate/silica and no Pt catalyst contact. This suggests that Pt might catalyze a reaction between oxygen and $(NH_4)_2SiP_4O_{13}$, leading to ammonium decomposition.

A control experiment shows that weight loss of the mixture of ammonium polyphosphate/silica and 20% Pd/carbon is only slightly more than that of pure ammonium polyphosphate/silica. So Pd might not catalyze the reaction between oxygen and $(NH_4)_2SiP_4O_{13}$.

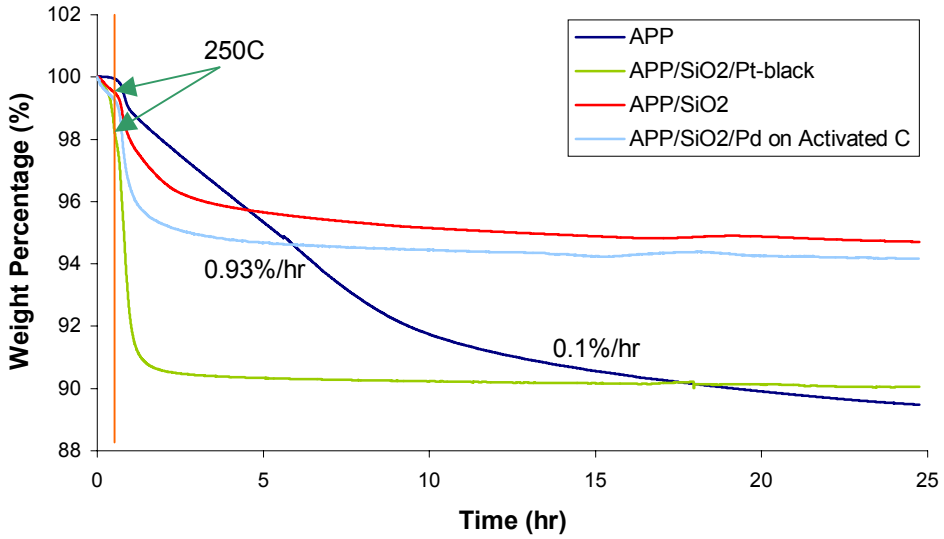

Fig. 5 Thermal Gravimetric Analysis (TGA) of pure ammonium polyphosphate and ammonium polyphosphate/silica at 250°C in an oxidizing atmosphere.

3.1.2 Fuel cell performance

Figure 6 shows fuel cell performance with H_2 and H_2/CO as fuels, and oxygen and air as the oxidant, using all inorganic hybrid proton conducting membrane based on ammonium polyphosphate and silica composite on a 25 μm Pd foil. The use of 5% CO balanced H_2 instead of pure H_2 has no negative effect on the fuel cell performance. The use of air instead of pure O_2 results in a decrease of OCV and cell performance. Increasing the air flow-rate from 100 sccm to 200 sccm causes an increase in the OCV from 0.66 V to 0.71 V.

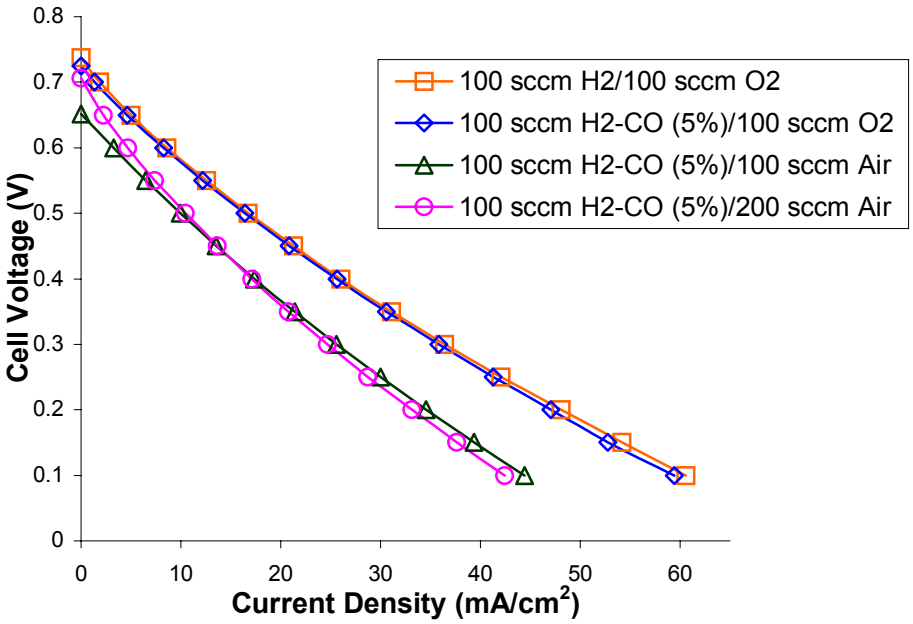

Fig. 6 Fuel cell performance using H_2 and H_2/CO versus air and oxygen.

Figure 7 shows a life time study at 400 mV in the presence of H_2/CO (5%) as fuel. The current density gradually increased, peaked at 10 hr, and then slowly decreased to ca. 21 mA/cm^2 at 25 hr.

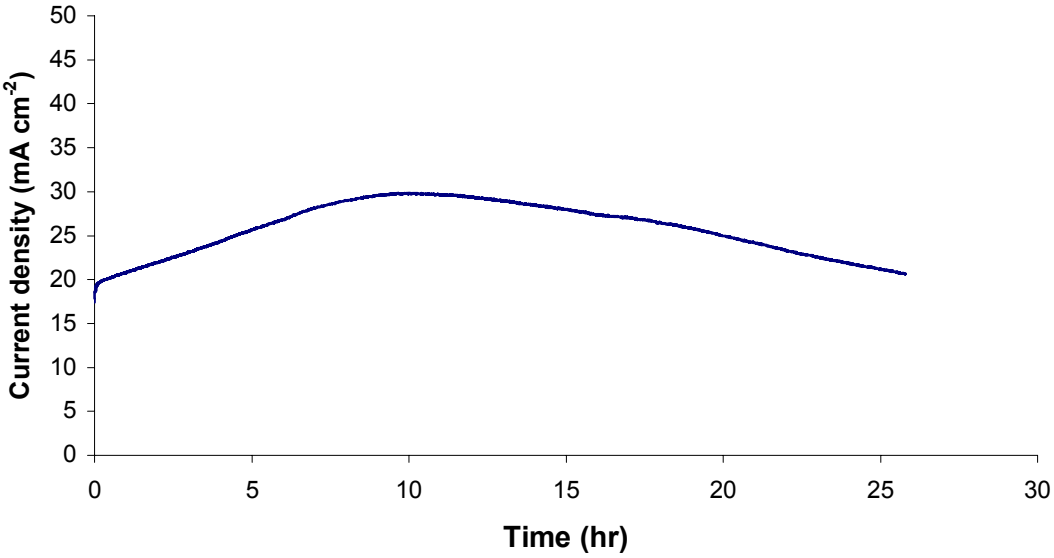

Fig. 7 Current density at 400 mV as a function of time at 250°C using H_2/5% CO as fuel.

The decay in current density (Fig. 7) and the TGA experiments suggested that water loss might be responsible for decay in current density at 250°C. This hypothesis was confirmed through XRD studies. Fig. 8 shows the XRD spectra of ammonium polyphosphate/silica coating on Pd foil before and after 2 days fuel cell operation at 250°C. Freshly prepared coating contains $(NH_4)_2SiP_4O_{13}$ as

the only crystalline phase [4]. After fuel cell operation at 250°C for two days, a portion of the $(NH_4)_2SiP_4O_{13}$ is converted to anhydrous SiP_2O_7 as evidenced by the changes of XRD diffraction patterns [5]. In order to understand the causes of conversion, a freshly prepared ammonium polyphosphate/silica coated Pd foil was assembled into fuel cell blocks with the coated side (cathode side) facing a Pt catalyzed GDL and uncoated side facing (anode side) a bare GDL. N_2 was purged through anode side while O_2 was purged through cathode side. The membrane was heated for 24 hrs, and then subjected to XRD analysis. Fig. 1 clearly shows conversion of $(NH_4)_2SiP_4O_{13}$ to anhydrous SiP_2O_7 upon heating. We suspect that Pt may catalyze a reaction between oxygen and $(NH_4)_2SiP_4O_{13}$, which then leads to ammonium decomposition.

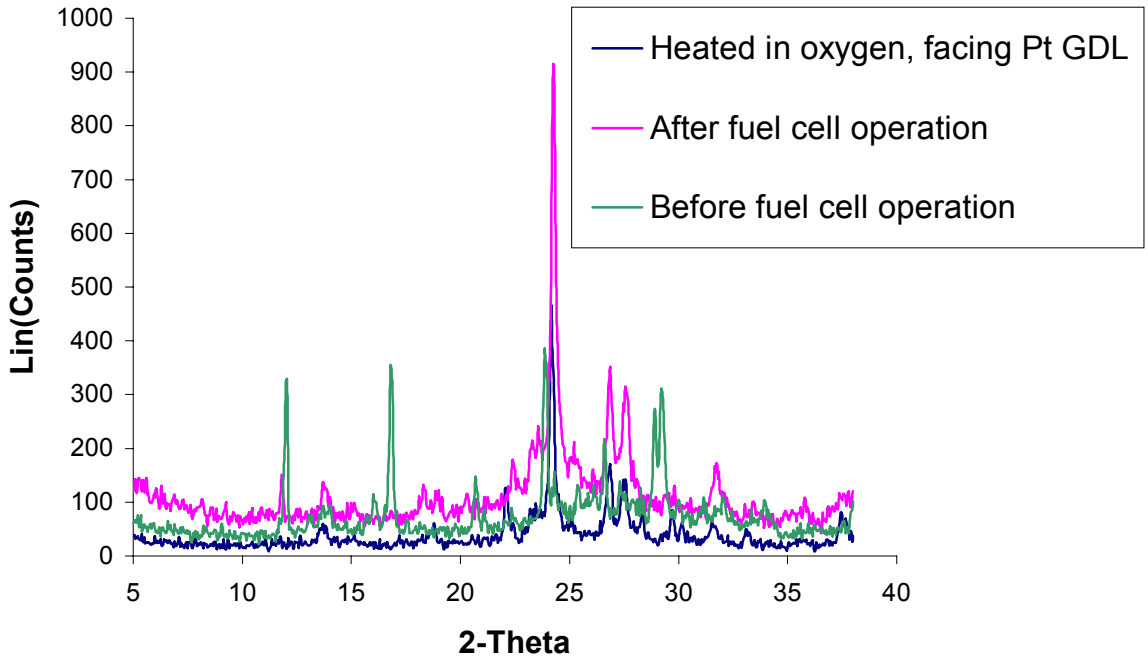

Fig. 8 XRD spectra of ammonium polyphosphate/silica coatings on Pd foil.

Impedance spectra were recorded by superimposing an ac signal on the cell in the constant dc voltage mode. Frequency of the ac signal applied was in the range of 0.1 Hz – 20 kHz and the amplitude of the ac signal was fixed at 10 mV. The impedance spectra were conducted as a function of cell voltage during steady state fuel cell operation. Figure 9 shows the potential dependent impedance data. The high frequency arcs show a much weaker potential dependence than the low frequency arcs. According to theoretical models, the low frequency arcs are related to the double layer capacitance of the electrode combined with the charge transfer resistance of the oxygen reduction reaction. The high frequency impedance arcs appear as a consequence of the presence of the distributed resistance inside the catalysts layer of the electrode, membrane resistance and contact resistance. The high frequency intercept determines the system resistance, which is ca. 4.5 Ω cm^2.

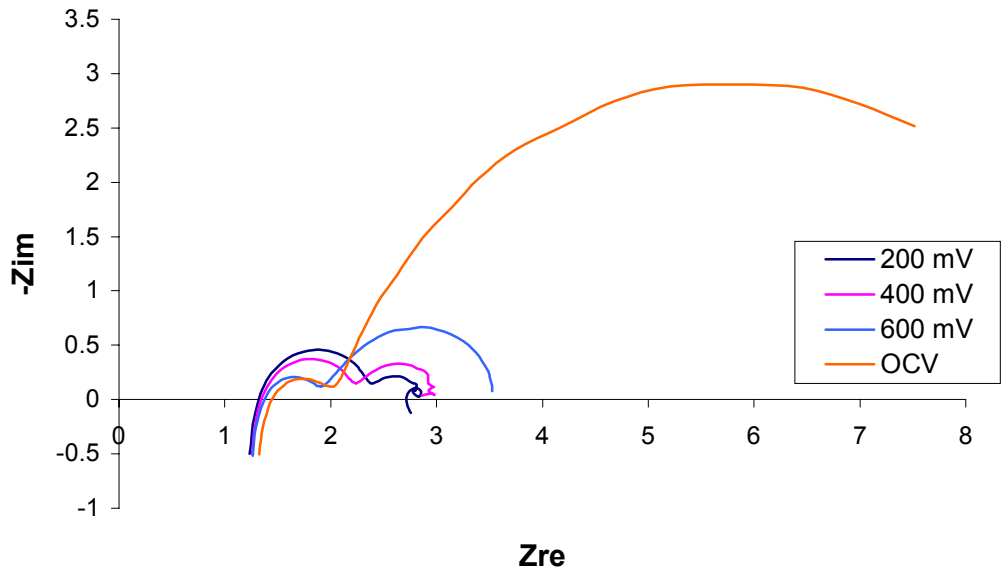

Fig. 9 Impedance plots for ammonium polyphosphate-silica/Pd membrane. Electrode area is 3.6 cm^2. Unit is Ω.

In the late stage of Phase I, commercially available ammonium polyphosphate (Clariant) was incorporated into the hybrid membrane system. Clariant manufactures and markets ammonium polyphosphate as a non-halogenated flame retardant. The material has a high molecular weight ($[NH_4PO_3]_n$, n > 1000), and relatively uniform particle size distribution (average particle size, 15 μm; (particles >100 μm, max. 0.2%; particles < 50 μm, min. 95%). Clariant ammonium polyphosphate is cheap and available in large quantities (25 kg 4-ply paper bag for $132). The availability of the commercially available product will permit NuVant to focus on optimization of the material with less concern about in-house preparative method parameters.

Clariant ammonium polyphosphate based electrode assemblies perform similarly to in-house prepared systems (Figure. 10). Although the data are only preliminary, the highest open circuit voltage has been obtained with Clariant (0.86 volts).

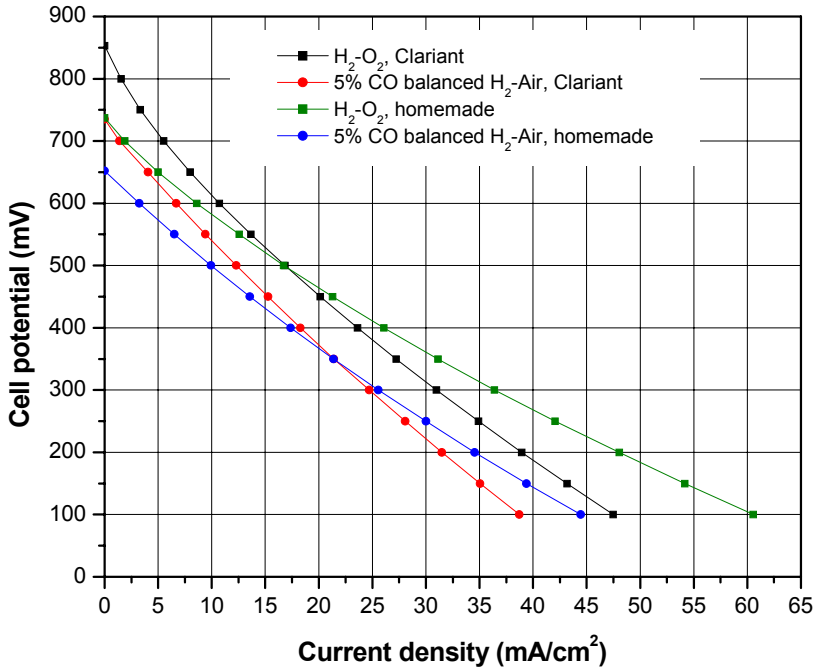

Fig. 10 I-V curves obtained at 250°C using Clariant ammonium polyphosphate. Pt catalysts are at the fuel cell anode and cathode.

3.2 BCN18 as EIPC materials

Many perovskite-type ceramics are known as high temperature proton conductors. Protons are incorporated into the structure by adsorption of water according to the following reaction:

$$H_2O(g) + V_o^{\cdot\cdot} + O_o^{\chi} \rightarrow 2OH_o^{\cdot}$$

Where $V_o^{\cdot\cdot}$ refers oxygen vacancy and O_o^{χ} refers to oxide ion at normal lattice site.

In the past, much attention has been paid to the ABO_3-type simple perovskites, particularly to the M^{3+} (rare earth)-doped $SrCeO_3$ and $BaCeO_3$. However, Ce-based perovskites suffer a deterioration of electrolytic quality upon exposure to severe atmospheres, e.g. they show considerable hole conduction at high temperature when exposure to oxygen and are readily decomposed into ACO_3 and CeO_2 in CO_2-containing atmosphere.

Recently, Nowick et al [6] reported another type of nonstoichiometric perovskite of the formula $A_3Ca_{1+x}Nb_{2-x}O_{9-\delta}$ (A = Sr, Ba), which shows promise as proton conductor upon exposure to H_2O vapor. These compounds have a wide band gap and are superior insulators without producing detectable residual electronic conduction under both oxidizing and reducing gas agents up to 1000ºC.

The nominal composition of the perovskite used in this study is $Ba_3Ca_{1.18}Nb_{1.82}O_{8.73}$. These types of materials have been synthesized by conventional ball milling, calcinations and high temperature sintering of mixtures of metal carbonates and metal oxides in stoichiometric ratio. However, these

methods are not amenable to the preparation of thin film. Thus we use sol-gel [7] and solution-particle [8] methods to prepare thin layers of BCN18 ceramics.

3.2.1 XRD of BCN18 bulk

Figure 11 is XRD spectrum of bulk BCN18, which shows a reasonably pure phase that matches the $Ba(Ca_{0.33}Nb_{0.67})O_3$ reference pattern (17-184).

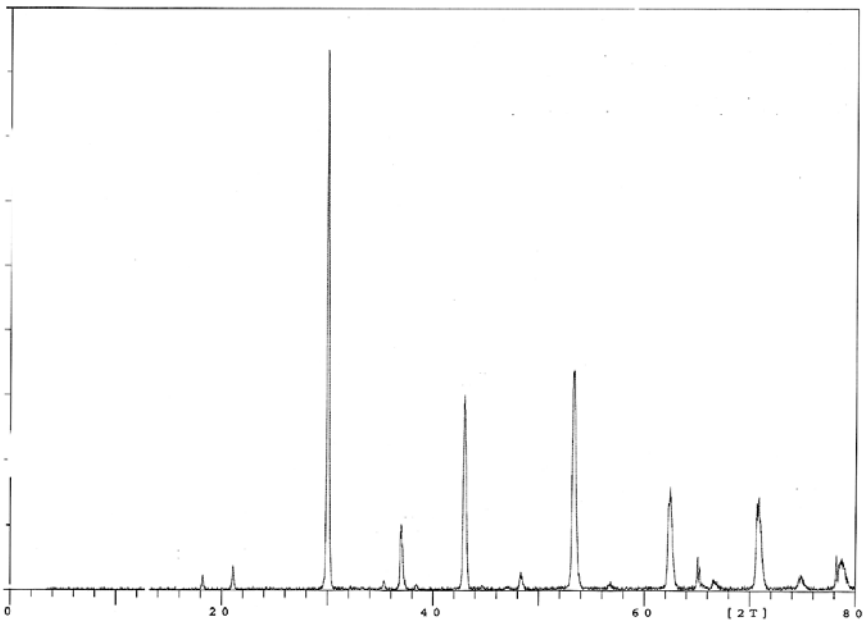

Fig. 11 XRD pattern of BCN18 bulk.

3.2.2 Dip-coating

The thickness of each BCN18 dip-coating layer is roughly 200 nm. Figure 2 shows the XRD pattern of Pd coated with 10 layers of BCN18. Both diffraction pattern of Pd foil and BCN18 coating were found in Fig. 12. The coating patterns roughly match that of bulk material, indicating that composition of coating is BCN18. (A new X-ray tube was installed before taking the XRD pattern of bulk BCN18. This might partially explain the slight difference between XRD patterns of bulk and coating.)

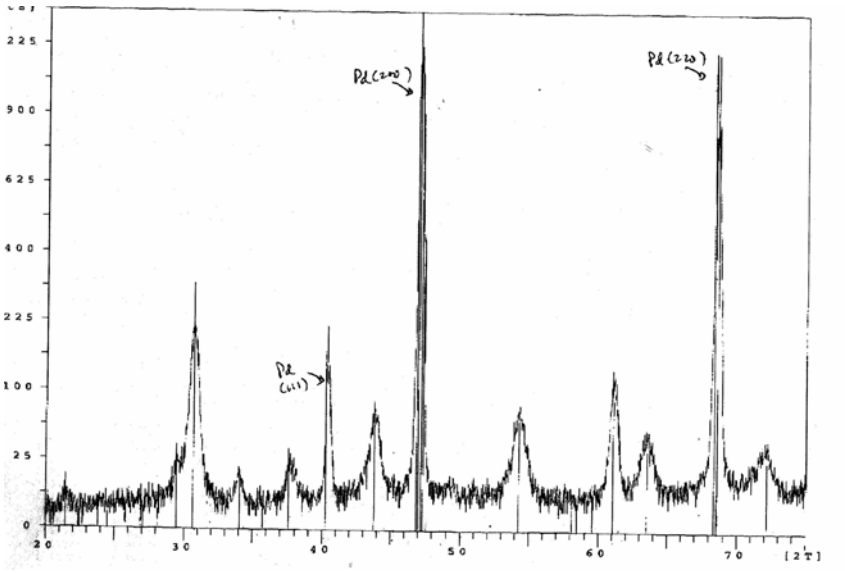

Fig. 12 XRD pattern of 10-layer BCN18 coated Pd foil. Peaks from Pd were identified.

Figure 13 shows the fuel cell performance of hybrid membrane made of BCN18 dip-coating. The sparger was set at room temperature. H_2 and O_2 were introduced at 200°C. Obvious OCV was observed at 300°C. One performance curve was collected at that temperature. The temperature was further increased to 350°C, and 3 more performance curves were collected. The final stable OCV is 0.93 V. From Figure 14, we can see that the fuel cell performance kept getting better in the three runs taken at 350°C. The third I-V curve appears approximately as straight line in accordance with Ohm's law. The membrane shows considerable stability. The fuel cell was operated for more than 2 hours without obvious failure. The same fuel cell was run again in the second day. The performance decayed a little bit, but was still within the same range as that of the first day.

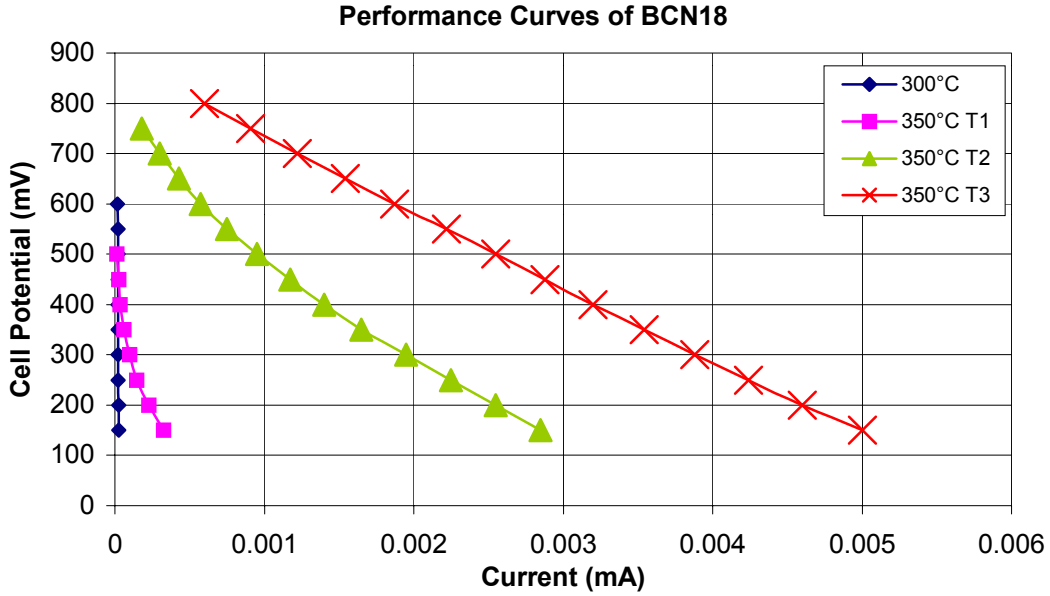

Fig. 13 Fuel cell performance of BCN18 coated Pd through dip-coating method.

3.2.3 Solution-particle method

The key to this method is to use ball milled BCN18. BCN18 powder without ball milling gave very rough surface. In contrast, coatings made of ball milled BCN18 powder looks very uniform and no visual particle agglomerates can be found. Figure 15 shows the fuel cell performance of two layers of BCN18 coated Pd foil at 315°C. Although the stable performance was achieved, the current density was low.

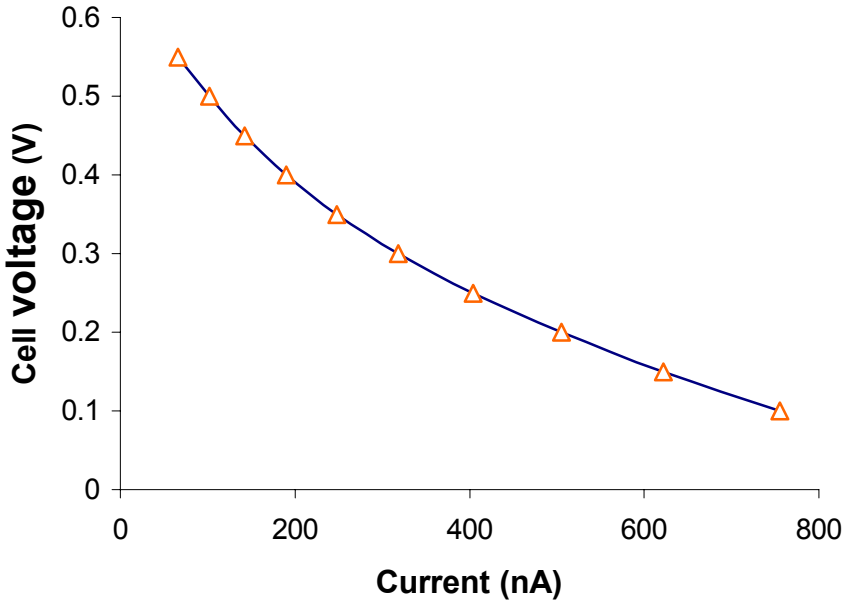

Fig. 14 Fuel cell performance of BCN18 coated Pd through particle-solution method.

3.2.4 Discussion and future directions

The current density of BCN18 based intermediate temperature fuel cell is too low to be practically meaningful. Combining the hydrogen permeability data, we believe that most of resistance came from BCN18 coatings. The conductivity (σ) of BCN18 bulk materials in the literature varied greatly in the range of 10^{-3} to 10^{-5} Ω/cm at 300°C. Assuming the membrane has the same proton conductivity as that of bulk, the resistance of BCN18 membrane can be calculated:

$$R = \frac{L}{\sigma A}$$

Where L is the thickness in cm, A is the area in cm^2.

For BCN18 membrane through dip coating, the thickness on each side of Pd foil is roughly 2 μm. The area of BCN18 membrane exposed to catalyst layer is 3.6 cm^2. Therefore, the calculated resistance should be in the range of 0.1 Ω to 10 Ω, which is much smaller than the resistance calculated from fuel cell performance curve (1.5×10^5 Ω). So it is obvious that the membrane material we prepared in Phase I has lower conductivity that that of bulk material. In Phase II, we will troubleshoot the issues identified in Phase I, and develop the coating method that will give a dense, crack-free thin film with the desired bulk proton conductivity.

3.3 Hydrogen permeability study

Little is known about hydrogen permeability under conditions relevant to intermediate temperature fuel cell operation. The setup shown in Figure 3 is designed to determine if there will be sufficient hydrogen flux through the membrane to support the current flux required for the intermediate temperature fuel cell operation.

3.3.1 Calibration

The setup was calibrated by sending a series of mixtures of known amount of H_2 and N_2 to GC. Figure 15 shows the calibration curve. Peak area is proportional to the volume fraction of H_2 in a wide range.

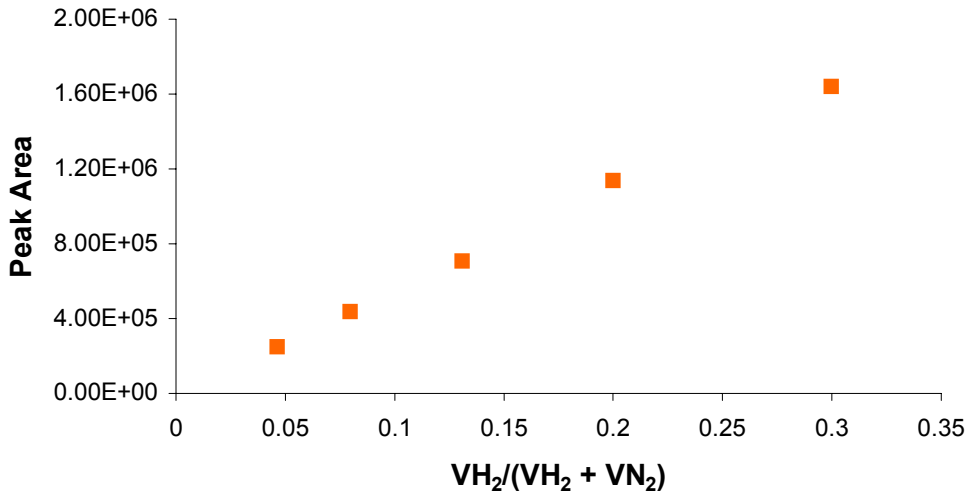

Fig. 15 H_2 calibration curve.

One of the first questions that must be answered regarding the future H_2 permeability experiments is: is the signal from the H_2 passing through the membrane or leaking through some other path? This question can be answered by using a gas mixture of H_2 and He as feed gas. If the signal is from H_2 passing through the membrane, then only H_2 signal will be observed because the metal foil has selectivity to H_2. If part of H_2 is from leaking, then both He and H_2 signal should be observed. Figure 16 shows the GC result of a mixture of 5.4 sccm He and 24 sccm H_2. We see two peaks that can be assigned to He and H_2, respectively. So the mixture of H_2 and He will be used as feed gas for the future experiments.

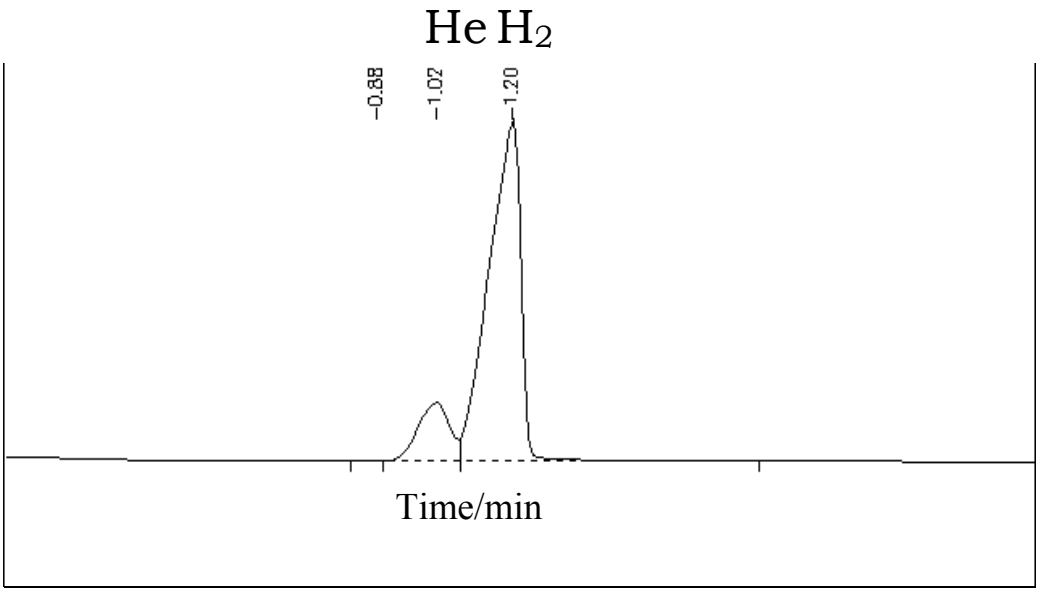

Fig. 16 GC result of a mixture of H_2 and He.

3.3.2 Hydrogen permeability study of Pd foil

Figure 17 shows the hydrogen signal through a Pd membrane at 250°C. Only pure H_2 peak was observed, indicating no leak or any other non-selective passing of feed gas. The area of the peak below corresponds to 17.6 sccm H_2 in the cathode exhaust, which means that 22% H_2 in the feed stream was transported across Pd membrane. Faradays' law demands 3.5 sccm/cm^2 H_2 to sustain 500 mA/cm^2. Thus the bulk phase of the support structure (Pd foil in this case) is not current limiting. It is likely that the primary source of impedance is associated with the bulk of the EIPC layer and/or EIPC/Pd interface. Strategies for reducing the resistance would be optimization of the coating process, operating at higher temperature and/or selection of an alternate EIPC.

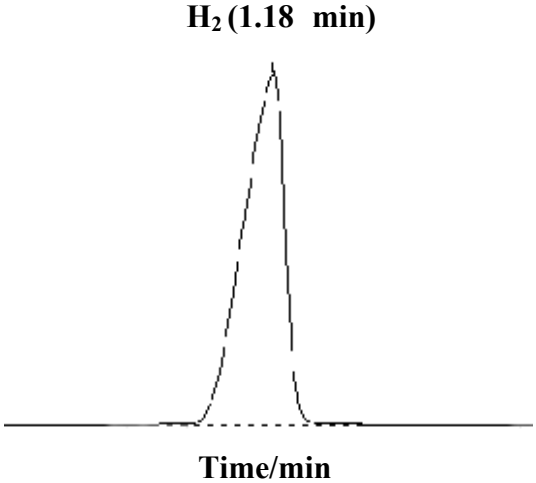

Fig. 17 GC results of cathode exhaust at 250°C.

Figure 18 shows H_2 flux as a function of membrane temperature. H_2 flow is seen to increase with the temperature.

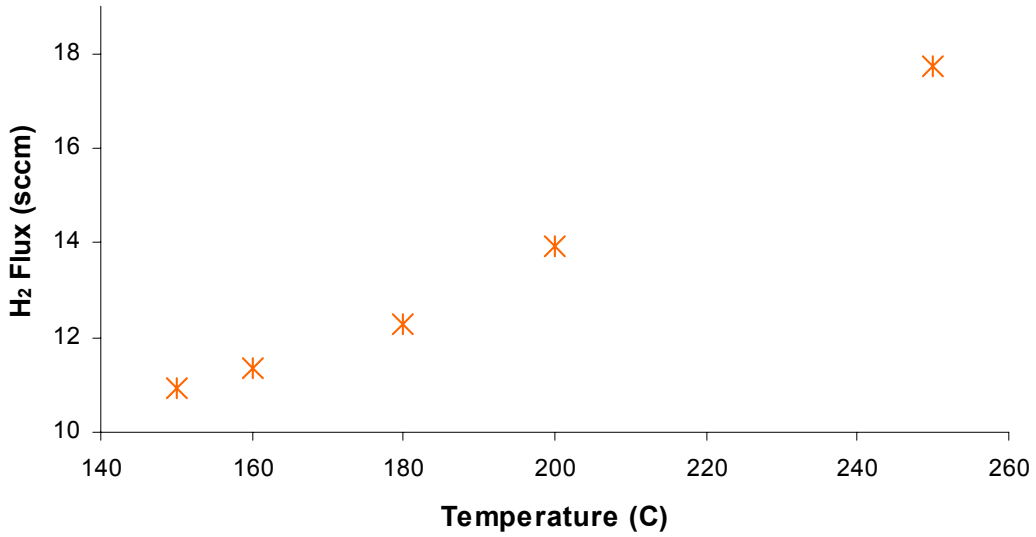

Fig. 18 H_2 flux as a function of membrane temperature.

3.3.3 Hydrogen permeability study of Pd coated V and V/Cu alloy membranes

3.3.3.1 Hydrogen permeability study of Pd coated V and V/Cu alloy membranes provided by Los Alamos National Labs (LANL)

The most important limitation of Pd or Pd alloys is their cost. Some cheaper alternatives are palladium-coated group Vb metal and alloys. Dr. Robert Dye of LANL provided Pd coated V and V/Cu foils (100nm Pd on 40 μm V or V/Cu foil). The fabrication method is described as follows. The foil was first cleaned with soap and water followed by a solvent rinse to remove surface oils. The foil was then mounted into a vacuum chamber, which was then pumped down to 10^{-6} torr. The foil was then cleaned using an argon ion gun to remove the native oxide layer. Without breaking the vacuum, layers of palladium of desired thickness were sputtered onto the front and back of the foil. Deposition thickness was monitored using a quartz crystal microbalance monitor, and the foil was kept at ambient temperature during cleaning and deposition.

Figure 19 shows the GC results for Pd/V/Pd foil at 250°C and 300°C. The H_2 permeation signal gradually increased over a period of 11 hr to 13.5 sccm at 250°C. Dr. Dye of LANL suggested that the induction period might be due to the relaxation of the interface, which is a time/temperature effect. Upon heating, the atoms at the interface move around some and lock into the lattice over a period of time. This assumption is confirmed by the hydrogen permeability study at 300°C, which shows a much shorter induction period (80% of maximum response was reached in 1 hr), and much higher hydrogen flux (45% H_2 in the feed stream was transported across composite foil). The hydrogen flux is enough to support 1 A/cm^2, confirming that the composite metal hydride can replace Pd as the support structure for electronically insulating proton conductor.

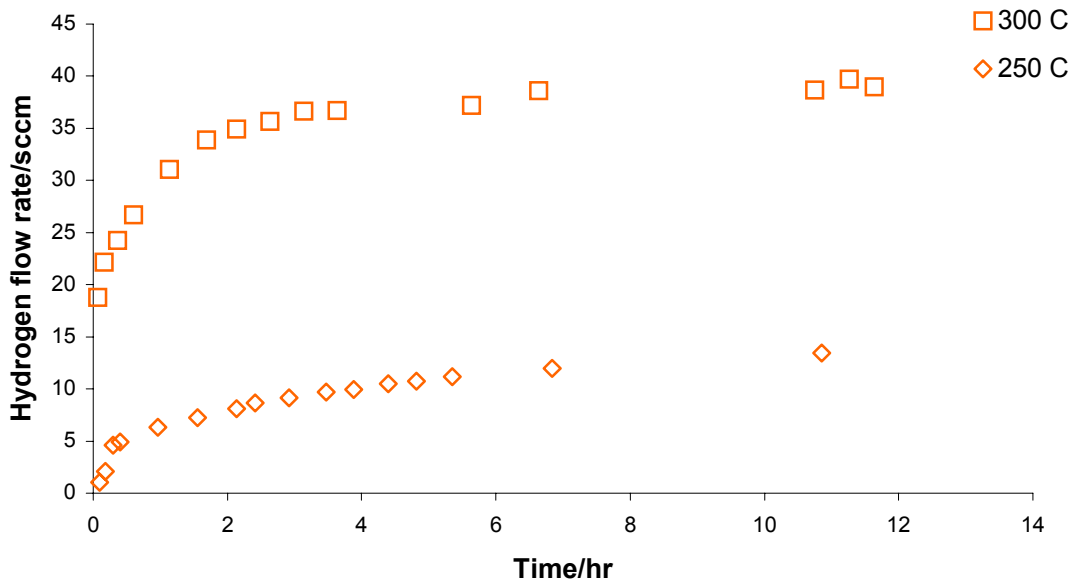

Fig. 19 H_2 flux through a Pd sputter coated V foil versus time at 250°C and 300°C.

Figure 20 shows the GC results for Pd coated V-Cu alloy foil at 250°C and 300°C. Although copper reduces the hydrogen solubility in vanadium, LANL reports that hydrogen embrittlement is less of a problem. The H_2 permeability through Pd coated V-Cu foil shows a relatively similar result as that of Pd coated V foil, and hydrogen flux reached 22 sccm at 300°C.

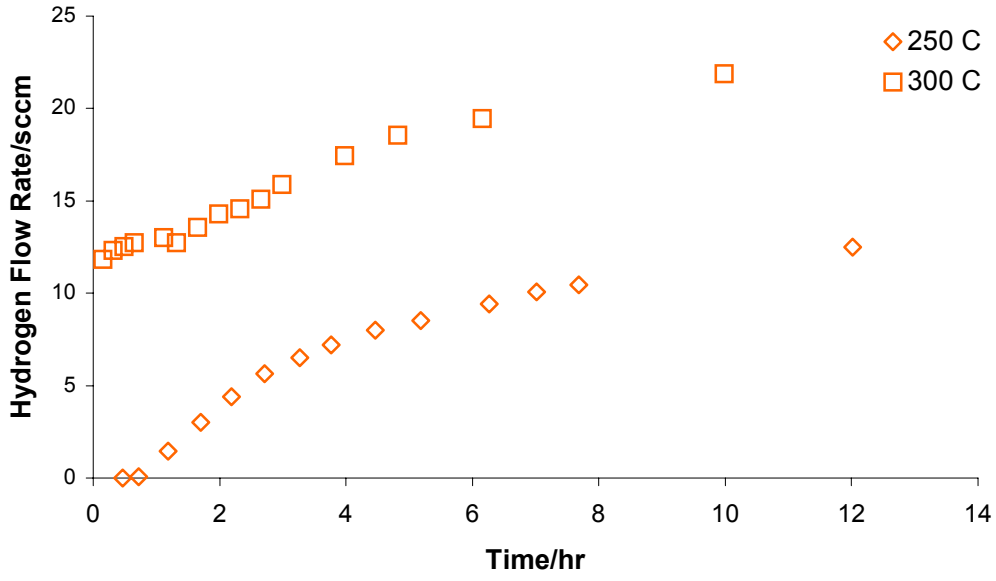

Fig. 20 H_2 flux through sputter deposited Pd/V-Cu/Pd foil versus time at 250°C and 300°C.

3.3.3.2 Hydrogen permeability study of Pd coated V made by electroplating

Electroplating method is a simple, low cost method that does not require sophisticated equipment. In a typical experiment, 3 × 3 cm vanadium foil (0.025 mm thick, 99.7%, Aldrich) was first

sonicated in hexane and acetone for 10 min. The foil was then etched in an acid bath (5% vol. HF acid (48 – 51%), 35% vol. HNO_3 acid) for 30 sec, and rinsed immediately with nanopure water. According to the weight loss, 0.6 μm of material on each side is estimated to be removed from the surface during etching. The freshly cleaned V foil was plated with desired amount of Pd on each side in a plating bath containing 10 g/L $Pd(NH_3)_4Cl_2$ and 8 g/L ammonium chloride (pH 8.5, adjusted by adding NH_4OH).) at 1.7 mA/cm^2.

Figure 21 shows the GC results at 250°C and 300°C. Steady state signal of 3.6 sccm H_2, was reached in 1.5 hr at 250°C for 40 nm Pd on 25 μm V foil. The data for 100 nm Pd on 25 μm V foil at 300°C shows much better results, and no induction period. However, hydrogen flux slowly decayed, then stabilized at 6 sccm in a period of 6 hr.

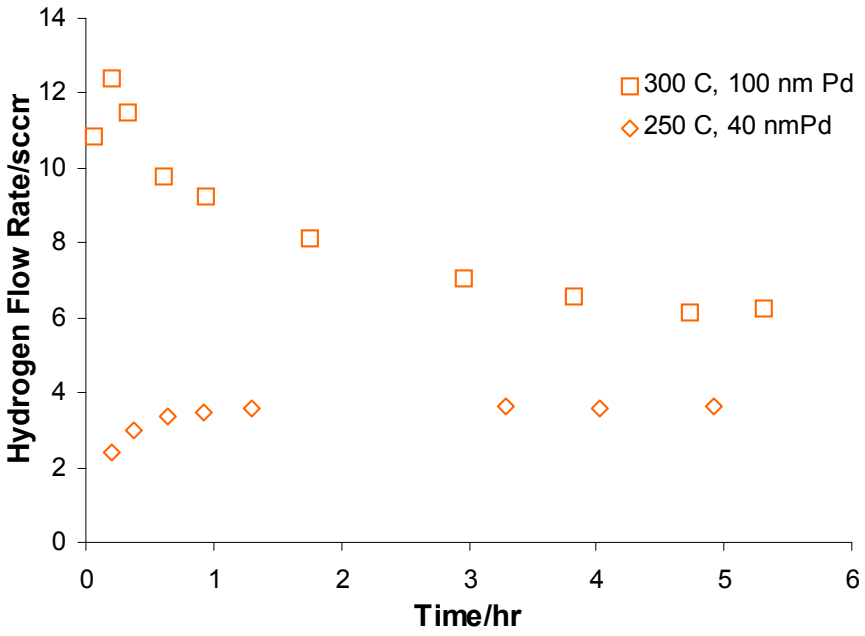

Fig.21 H_2 permeability study of electroplated Pd/V/Pd foils versus time at 250°C and 300°C. 40 nm Pd on 25 μm V foil was used at 250°C, and 100 nm Pd on 25 μm V foil was used at 300°C.

4 Conclusion

In Phase I, we demonstrate the feasibility of making supported electronically insulating, proton conducting inorganic thin films on metal hydride foils for intermediate temperature fuel cell electrolytes. Free standing, all inorganic composite membranes consisting of 2 – 20 μm inorganic films on 25 μm Pd foil have been successfully prepared and used as proton conducting membrane for intermediate fuel cell application. On the contrary, it is very difficult to prepare a mechanically strong inorganic electrolyte membrane with the same thickness using conventional methods. The fuel cell based on the supported membranes shows complete tolerance to 5% CO balanced hydrogen with considerable stability at 250°C. We also demonstrated that Pd coated V foils are viable candidates for replacement of Pd as the supported structure for proton conducting electrolytes.

5 Participating Scientific Personal

Yipeng Sun, Senior Research Scientist, Principal Investigator
Renxuan Liu, Senior Research Scientist
Upendra Rao, Research Scientist
Eugene Smotkin, Chief Executive Officer

---

1 P. W. Huber, M. P. Mills, *Digital Power Report*, 6-7, Gilder Publishing, Housatonic MA (September, 2000)
2 D. S. Cameron, G. A. Hards, D. Thompsett, in *Proceedings of the Workshop on Direct Methanol-Air Fuel Cells*, A. R. Landgrebe, R. K. Sen, D. J. Wheeler, Eds. , Electrochem. Soc. Proc. 92-14, 1992, pp. 10-23.
3 T. Kenjo, Y. Ogawa, Solid State Ionics 76 (1995) 29.
4 Averbuch-Pouchot, M., Durif. J Solid State Chem, 18 (1976), 391.
5 Chenuit et al. J Solid State Chem, 68(1987), 94.
6 A.S. Nowick, Y. Du, *Solid State Ionics 77*, 137, **1995**.
7 B. Gross, et al, *Solid State Ionics*, *125*, 107, **1999**.
8 Burtrand I. Lee, *et al*, *Materials Research Bulletin*, *36*, 1065, **2001**.